Effect of Silicon Dioxide on Crystallization and Melting Behavior of Polypropylene

Minjie Chen, Guohua Tian, Yong Zhang, Chaoying Wan, Yinxi Zhang

Research Institute of Polymer Materials, Shanghai Jiao Tong University, 200240 Shanghai, People's Republic of China

Received 3 June 2005; accepted 3 June 2005
DOI 10.1002/app.23315
Published online 2 February 2006 in Wiley InterScience (www.interscience.wiley.com).

ABSTRACT: The crystallization and melting behavior of isotactic polypropylene (iPP) and polypropylene copolymer (*co*-PP) containing silicon dioxide (SiO_2) were investigated by differential scanning calorimeter (DSC). SiO_2 had a heterogenous nucleating effect on iPP, leading to a moderate increase in the crystallization temperature and a decrease in the half crystallization time. However, SiO_2 decreased the crystallization temperature and prolonged the half crystallization time of *co*-PP. A modified Avrami theory was successfully used to well describe the early stages of nonisothermal crystallization of iPP, *co*-PP, and their composites. SiO_2 exhibited high nucleation activity for iPP, but showed little nucleation activity for *co*-PP and even restrained nucleation. The iPP/SiO_2 composite had higher activation energy of crystal growth than iPP, indicating the difficulty of crystal growth of the composite. The *co*-PP/SiO_2 composite had lower activation energy than *co*-PP, indicating the ease of crystal growth of the composite. Crystallization rates of iPP, *co*-PP, and their composites depended on the nucleation. Because of its high rate of nucleation, the iPP/SiO_2 composite had higher crystallization rate than iPP. Because of its low rate of nucleation, the *co*-PP/SiO_2 composite had lower crystallization rate than *co*-PP. © 2006 Wiley Periodicals, Inc. J Appl Polym Sci 100: 1889–1898, 2006

Key words: polypropylene; crystallization; differential scanning calorimetry

INTRODUCTION

Inorganic fillers are widely used in the polymer industry to improve the mechanical properties of polymers, such as heat distortion temperature and hardness. Compared with conventional composites based on micron-sized inorganic fillers, nanocomposites based on nanoscale fillers, such as calcium carbonate, clay, and silica, have drawn great attention because of the improved mechanical properties.[1–5] To achieve this improvement, the nanoscale fillers must be fully dispersed throughout and connected to the matrix after using an appropriate modifier to increase the hydrophobicity of the fillers.[6–8]

Incorporation of nanoscale fillers is a promising approach to increase stiffness or toughness of isotactic polypropylene (iPP), with satisfied results.[9–11] The incorporation of $CaCO_3$ nanoparticles in iPP could increase the impact strength by about 300%.[9] The tensile strength and elongation at break of iPP could be simultaneously increased after the incorporation of polymer-grafted silicon dioxide.[10] A small amount of polyoxyethylene nonyphenol has been used to improve the dispersion of $CaCO_3$ particles in iPP and increase the notched Izod impact strength significantly, without compromising the tensile strength and modulus very much.[11]

iPP is a semicrystalline polymer and it is easy to crystallize.[12] Nanoscale filler/iPP composites have different crystalline structure from iPP.[12] $CaCO_3$ nanoparticles have a nucleating effect on iPP and could decrease the crystal size and increase the tensile modulus of iPP by about 85%.[9] The introduction of $CaCO_3$ nanoparticles in iPP matrix resulted in small and imperfect iPP crystals, decreased crystal growth rate, and induced formation of β-form crystal.[11] Nano-silicon dioxide (SiO_2) could increase the crystallization rate and shorten the half-time of crystallization of iPP.[13]

Copolymer-PP (*co*-PP) contains a small amount of ethylene monomer units. It has lower melting temperature and higher impact strength than those of iPP. To our knowledge, few publications are concerned with *co*-PP/SiO_2 composites. Because of the presence of ethylene monomer units in *co*-PP, *co*-PP/SiO_2 composites should have different crystallization behavior and crystal structure from iPP/SiO_2 composites, which might affect the mechanical properties of composites in turn. In addition, *co*-PP has drawn increasing attention for its application in polymer composites. In this study, *co*-PP/SiO_2 composites were prepared and the crystallization and melting behavior of *co*-PP/SiO_2 nanocomposites were investigated and compared with that of iPP/SiO_2 nanocomposites.

Correspondence to: Y. Zhang (yong_zhang@sjtu.edu.cn).

EXPERIMENTAL

Materials

co-PP (Moplen RP344R, injection grade) was purchased from Basell Polymirae (Korea) with melt flow index (MFI) of 30 g/10 min at 230°C (ASTM D1238). iPP (1304E1, injection grade) was purchased from Exxon Mobile with MFI of 11 g/10 min at 230°C (ASTM D1238). SiO_2 nanoparticles (Degussa VN3 pH 6.2, BET = 175 m^2/g) were supplied by Red Avenue Chemical. The size of SiO_2 was in the range of 30–80 nm. SiO_2 nanoparticles were blended with 2 wt % A-171 (vinyl trimethoxysilane)silane coupling agent in a high-speed internal mixer before use.

Preparation of nanocomposites

SiO_2 nanoparticles were dried in an oven at 70°C for 12 h before melting extrusion. PP and SiO_2 (3 wt %, based on the PP matrix) were blended in a twin-screw extruder with the temperature profiles of 200, 200, 210, 210, and 200°C (denoted from the inlet hopper to the end of screws), and the extruded strands were chopped into granules and dried at 100°C for 5 h.

Nonisothermal crystallization and melting analysis

Nonisothermal crystallization was carried out on a Perkin–Elmer Pyris-1 DSC. A sample of 5–7 mg was heated up first to 200°C rapidly and kept for 5 min to eliminate the thermal history. Then, the sample was cooled down to 20°C at a cooling rate of 2.5, 5, 10, 20, or 40°C/min, respectively. At last, the sample was subsequently reheated to 200°C at the heating rate of 10°C/min. The heat flow as a function of temperature was recorded to analyze the nonisothermal crystallization and melting process of PP/SiO_2 composite.

Wide angle X-ray diffraction

A sample was cut from a dumb-bell bar and scanned with a speed of 4°/min at ambient temperature, using a X-ray diffractometer (Bruker AXS DE Advance, Bruker, Germany) with Cu $K\alpha$ radiation (λ = 0.154 nm), at a generator voltage of 40 kV and a current of 30 mA.

RESULTS AND DISCUSSION

Effects of SiO_2 nanoparticles on the crystallization and melting behavior of iPP and *co*-PP

The crystallization exotherms of iPP/SiO_2 and *co*-PP/SiO_2 composites are shown in Figure 1. SiO_2 increased the crystallization temperature of iPP from 117.7 to 121.3°C. Most inorganic fillers can always act as nucleating agents for iPP and increase the crystallization

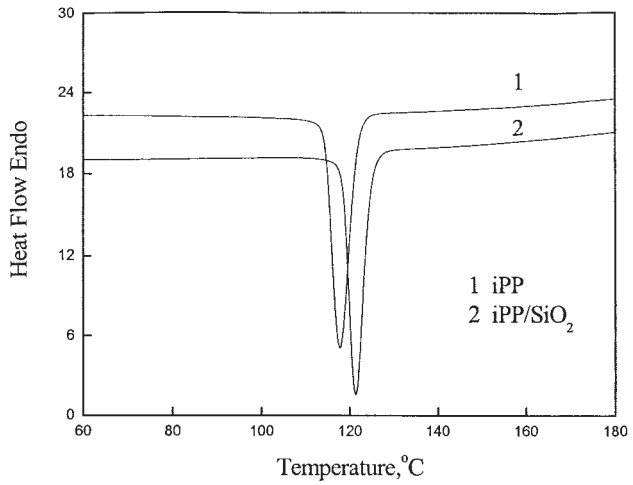

(a)

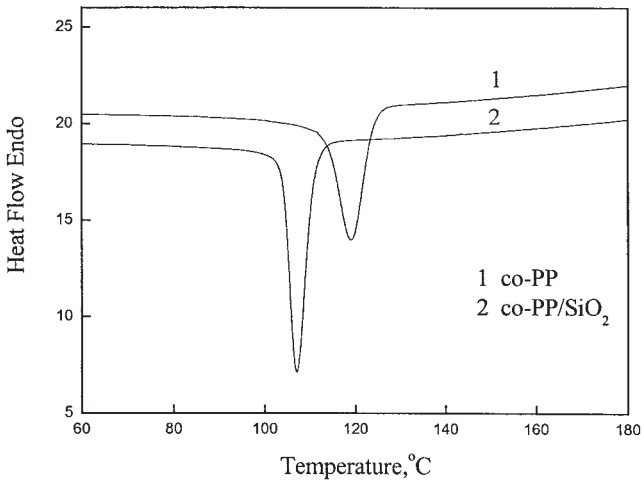

(b)

Figure 1 DSC cooling curves of iPP (a) and *co*-PP (b), and their SiO_2 composites at a cooling rate of 10°C/min.

temperature.[9,13,14] An abnormal phenomenon can be seen in Figure 1(b), that is, SiO_2 decreased the crystallization temperature of *co*-PP from 119.2 to 107.0°C. The molecules of *co*-PP contain a small amount of ethylene structural units distributed random along the main molecule chains and some short segments with low isotacticity. Because SiO_2 nanoparticles have large surface area and high surface free energy, the short segments with low isotacticity of *co*-PP chain should prefer to be absorbed on the filler surface. If so, the mobility of *co*-PP molecular chains would be restricted, leading to the crystallization ability and temperature decrease. The phenomena were also reported in Ref. 17. Nucleation and absorption are two factors from the filler side affecting the behavior of crystallization. Nucleation can accelerate the crystallization, while absorption can retard the crystallization.[15] The

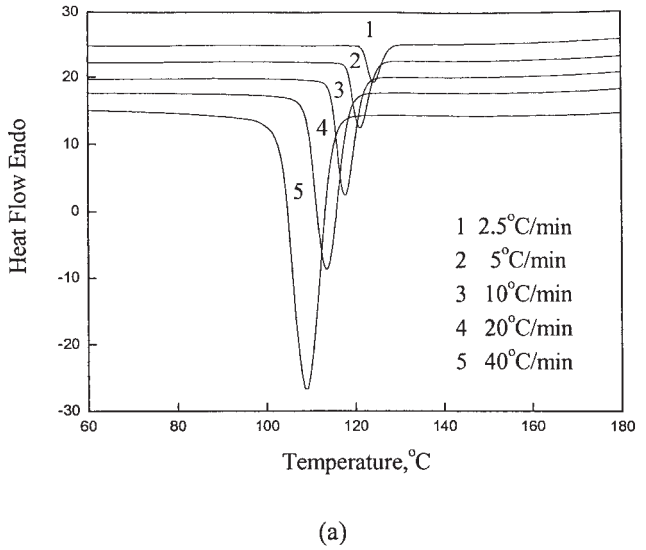

Figure 2 DSC curves of nonisothermal crystallization at different cooling rates of iPP (a) and iPP/SiO_2 (b).

aforementioned experimental results indicate that the heterogeneous nucleation of SiO_2 played a decisive role for the crystallization of iPP composite, while the absorption effect of SiO_2 played a decisive role for the crystallization of *co*-PP composite.

Figures 2 and 3 show the heat flow curves during the nonisothermal crystallization of iPP and *co*-PP at different cooling rates, respectively. The crystallization and melting data of iPP, *co*-PP, and their composites are listed in Table I. The crystallization temperatures of all the materials shift to lower temperatures with the increasing cooling rate. At high cooling rates, the polymer molecules are difficult to move and fold and the crystallization is hindered, leading to a high degree of supercooling.[13]

Figure 4 shows subsequent reheating DSC curves of iPP and iPP/SiO_2, after crystallized at different cooling rates. With increase in cooling rate, the melting peaks shift to lower temperatures as shown in Figure 4(a), implying the reduction of lamellar thickness of iPP. When the cooling rate is as high as 40°C/min, there is a shoulder peak on the right side of main melting peak, which is attributed to the re-crystallization of originally formed imperfect crystals during the fast cooling process.[16] During the subsequent reheating process, these imperfect crystals can re-crystallize into larger crystals with higher melting temperature.[17] As for iPP/SiO_2 composite shown in Figure 4(b), the lamellar thickness of iPP also reduces with the increase in cooling rate. Nevertheless, no re-crystallization peak can be observed on the melting curve of iPP/SiO_2 composite at a cooling rate of 40°C/min. It can be explained from the good crystallization ability

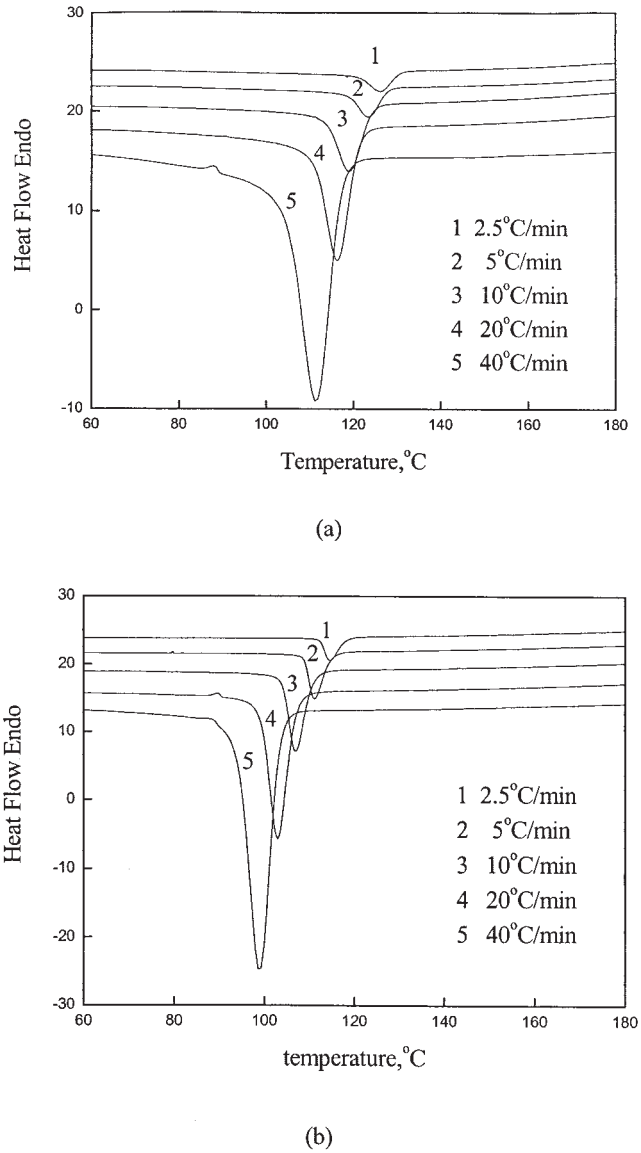

Figure 3 DSC curves of nonisothermal crystallization at different cooling rates of *co*-PP (a) and *co*-PP/SiO_2 (b).

TABLE I
The Crystallization and Melting Data of iPP and *co*-PP

Cooling rate (°C/min)	T_c (°C)	ΔH_c (J/g)	T_m (°C)	ΔH_m (J/g)	X_c (%)
iPP					
2.5	124.2	100.8	163.1	104.3	49.9
5	121.1	99.4	162.8	101.6	48.6
10	117.7	97.7	160.3	100.2	47.9
20	113.6	93.7	159.9	97.2	46.5
40	109.3	91.2	158.8	94.6	45.3
iPP/SiO_2					
2.5	127.7	99.3	163.8	99.6	47.7
5	124.8	97.5	162.1	99.4	47.6
10	121.3	94.1	162.1	96.4	46.1
20	117.3	92.7	161.6	92.2	44.1
40	113.9	89.5	160.3	92.0	44.0
co-PP					
2.5	126.2	63.3	150.7	66.5	—
5	123.5	58.8	149.5	63.9	—
10	119.2	58.7	148.9	61.8	—
20	116.3	57.5	149.2	58.9	—
40	111.2	56.9	147.3	57.8	—
co-PP/SiO_2					
2.5	114.2	69.9	147.0	70.7	—
5	111.2	68.2	145.8	67.5	—
10	107.0	66.8	144.8	62.5	—
20	103.0	64.7	144.0	59.2	—
40	98.6	62.9	142.5	57.9	—

T_c and T_m are the peak temperatures of crystallization and melting, respectively; crystallinity: $X_c = \Delta H_m/\Delta H_m^0$ where $\Delta H_m^0$is 209 J/g for the completed crystallized iPP.

of iPP in the iPP/SiO_2 composite at higher temperature because of the effect of heterogeneous nucleation of SiO_2. The crystallinities of iPP were calculated from the melting heat and are shown in Table I. With the increasing cooling rate, the iPP molecules do not have enough time to crystallize. That is why the crystallinity of iPP decreases with the increasing cooling rate.

Figure 5(a) shows subsequent reheating DSC curves of neat *co*-PP, after crystallized at different cooling rates. With the increasing cooling rate, the melting peaks move to lower temperatures, indicating the reduction of lamellar thickness of *co*-PP. To the left side of main melting peaks, there are strong and wide shoulder peaks, especially at low cooling rates (<10°C/min). Introduction of ethylene monomer into the polypropylene chains decreases the chain regularity and there are some short segments on the main chains.[17] These shoulder peaks represent the melting of small crystals related to the short segments, which should have low melting temperatures. With the increasing cooling rate, the short segments do not have enough time to crystallize and the shoulder peaks become weaker.

Figure 5(b) shows the subsequent reheating DSC curves of *co*-PP/SiO_2 composite crystallized at different cooling rates. The shoulder peaks on the left side of main melting peaks are weaker with respect to *co*-PP. Because SiO_2 nanoparticles restrict the movement of short segments, the crystals formed by the short segments become smaller in size and less perfect. At high cooling rates (>10°C/min), the short segments do not have enough time to crystallize and then there are not obvious shoulder peaks on the left side of the main melting peaks. In contrast to *co*-PP, the *co*-PP/SiO_2 composite has shoulder peaks appeared on the right side of the main melting peaks and their intensity increases with the increasing cooling rate. These shoulder peaks should be resulted from the re-crystallization of originally formed imperfect crystals, during the subsequent reheating process. The higher the cooling rate is, the less perfect the formed crystals are.

Because SiO_2 nanoparicles can decrease the crystallization temperature of *co*-PP, there are some defects

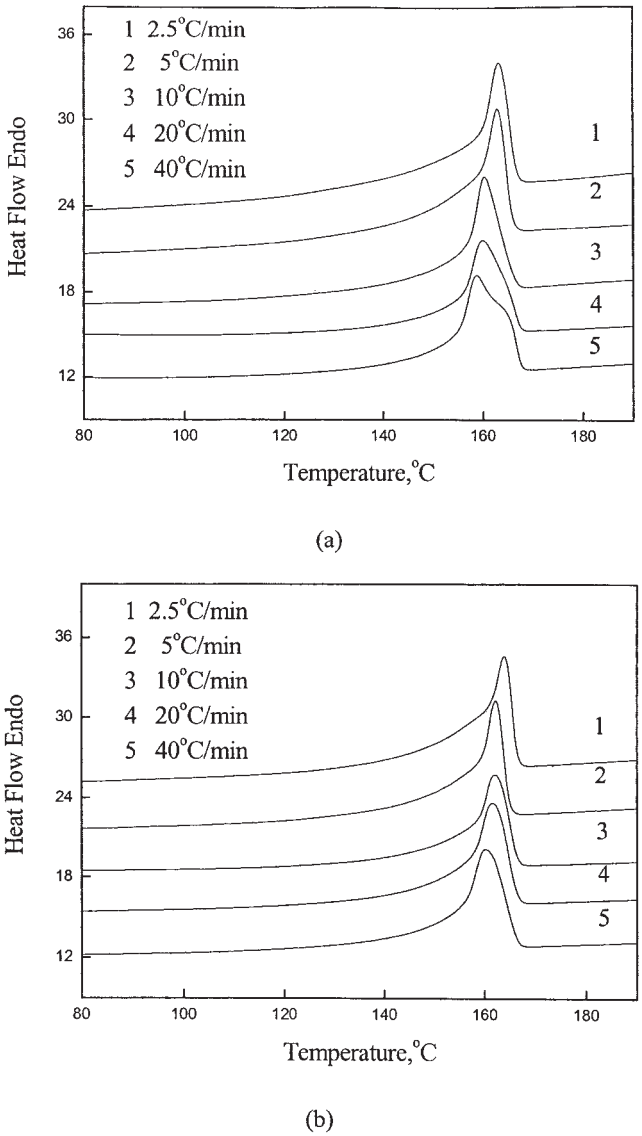

Figure 4 Subsequent reheating DSC curves (heating rate of 10°C/min) of iPP (a) and iPP/SiO_2 (b), after crystallized at different cooling rates.

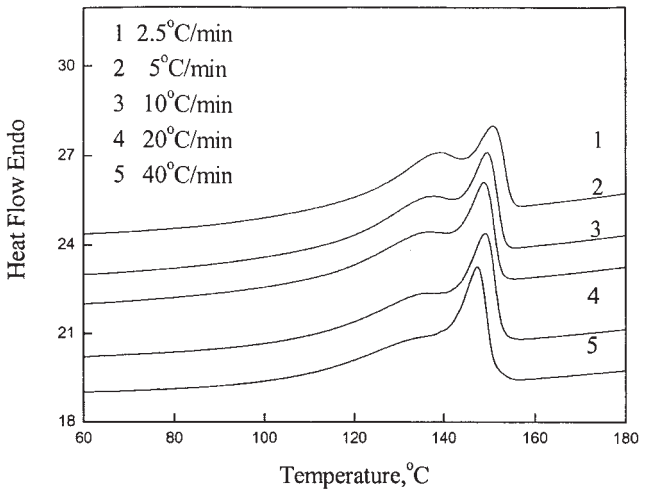

Figure 5 Subsequent reheating DSC curves (reheating rate of 10°C/min) of *co*-PP (a) and *co*-PP/SiO_2 (b), after crystallized at different cooling rates.

in the *co*-PP crystals. The melting temperatures of *co*-PP/SiO_2 composite are lower than that of *co*-PP (Table I). Because the standard heat of crystallization of *co*-PP is not available, the crystallinity of *co*-PP composite cannot be calculated. Judged from the data of ΔH_m (Table I), the crystallinities of *co*-PP and *co*-PP/SiO_2 composite decrease with the increasing cooling rate.

Nonisothermal crystallization kinetics of iPP/SiO_2 and *co*-PP/SiO_2 composites

To further analyze the nonisothermal crystallization process, the nonisothermal crystallization kinetics of iPP/SiO_2 and *co*-PP/SiO_2 composites were investigated. Just like isothermal analysis, the nonisothermal crystallization can also be directly analyzed by the Avrami equation[14]:

$$X(t) = 1 - \exp(Z_t t^n) \quad (1)$$

where $X(t)$ is the relative crystallinity at crystallization time t; n, the Avrami exponent; and Z_t, the crystallization rate constant. Equation (1) can be changed into logarithmic form as follows:

$$\ln[-\ln(1-X(t))] = n \ln(t) + \ln(Z_t) \quad (2)$$

Applying the Avrami theory, a plot of $\ln[-\ln(1-X(t))]$ versus $\ln(t)$ should yield a straight line with slope n and intercept Z. Jeziorny[18] considered Z_t should be modified to the following equation:

$$\ln Z_c = \ln Z_t / \phi \quad (3)$$

where ϕ is a cooling rate. Figures 6 and 7 show plots of $\ln[-\ln(1-X(t))]$ versus $\ln(t)$ for iPP and *co*-PP composites, respectively. The kinetics parameters of nonisothermal crystallization are summarized in Table II.

At the early stage of crystallization, $\ln[-\ln(1-X(t))]$ is in a good linear relation with $\ln(t)$, indicating that the modified Avrami equation is suitable for these composites. From Table II, it can be seen that the half crystallization time ($t_{1/2}$) of composite decreases with increase in ϕ. At a given cooling rate, $t_{1/2}$ of iPP/SiO_2 is lower than that of iPP, indicating that SiO_2 nanoparticles could accelerate crystallization rate of iPP. However, at a given cooling rate, $t_{1/2}$ of *co*-PP/SiO_2 is higher than that of *co*-PP, indicating that SiO_2 nanoparticles could reduce crystallization rate of *co*-PP. Z_c increases with increasing ϕ for all the composites. High cooling rate is favorable for crystallization and can increase the crystallization rate constant.[14] The average value of n is 1.85 for iPP, 1.85 for iPP/SiO_2, 1.46 for *co*-PP, and 1.62 for *co*-PP/SiO_2. According to the analyses results of modified Avrami equation, there are no distinct differences in mechanism of nucleation and crystal growth style for the composites within a given range of n values.[13] Because of the nucleation effect of SiO_2 nanoparticles, the crystallization rate of iPP/SiO_2 composite is higher than that of neat iPP. Because of the absorption of SiO_2 nanoparticles, the crystallization rate of *co*-PP/SiO_2 is lower than that of neat *co*-PP.

Nucleating activity

The iPP/SiO_2 composite has higher crystallization rate and T_c than those of iPP, which arises from the heterogeneous nucleation effect of SiO_2 nanoparticles.[14]

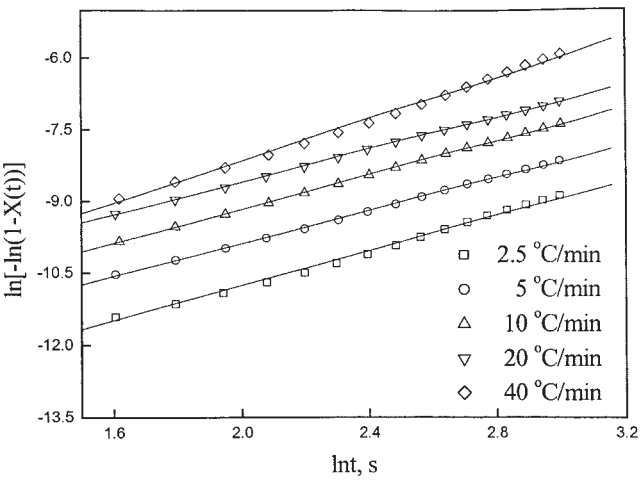

(a)

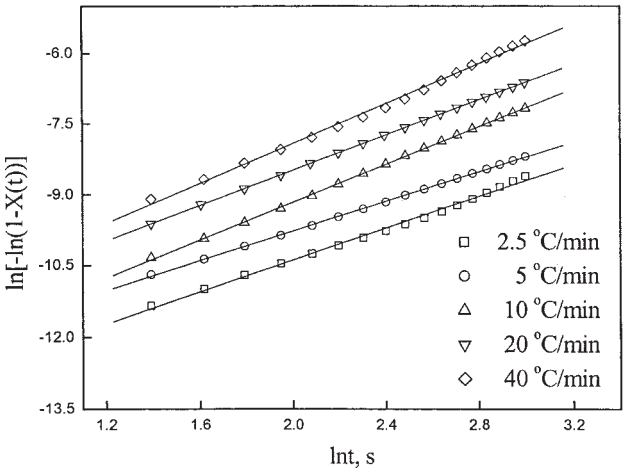

(b)

Figure 6 Plots of ln[−ln(1−$X(t)$)] versus ln t for nonisothermal crystallization of iPP (a) and iPP/SiO_2 (b).

The *co*-PP/SiO_2 composite has lower crystallization rate and T_c than those of *co*-PP, and the nucleation effect of SiO_2 nanoparticles in *co*-PP/SiO_2 composite is not obvious. The nucleating activity of SiO_2 nanoparticles depends on the PP type of PP composites. Dobreva[19,20] proposed a method to calculate the nucleating activity of a filler. In the case of study of the nonisothermal crystallization process, the following relationships were proposed[19,20]:

$$\log\phi = \text{cont} - \frac{B}{2.3\Delta T_p^2} \tag{4}$$

where ΔT_p reflects supercooling extent and equals to $T_m^0 - T_p$ (T_m^0 is the equilibrium melting temperature and T_p is the peak temperature of crystallization). B, a parameter, can be calculated from the following equation:

$$B = \omega\frac{\sigma^3 V_m^2}{3kT_m\Delta S_m^2 n} \tag{5}$$

where V_m is the molar volume of the polymer, ΔS_m is the entropy of melting, k is the Boltzman constant, σ is the specific surface energy, and ω is a geometrical factor.

The nucleating activity of the filler, ε, is defined as the ratio between the three-dimensional work of nucleation with and without filler (A_f and A_0, respectively). If the filler is extremely active for nucleation, ε approaches 0. And for absolutely inert particles ε is 1. If ε exceeds 1, the filler not only has no the heteroge-

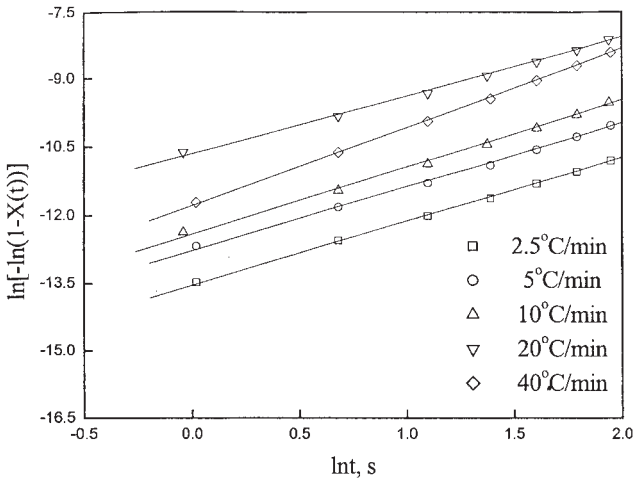

(a)

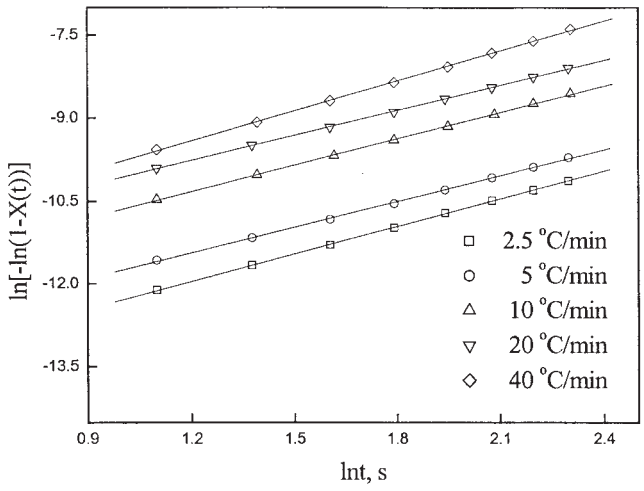

(b)

Figure 7 Plots of ln[−ln(1−$X(t)$)] versus ln t for nonisothermal crystallization of *co*-PP (a) and *co*-PP/SiO_2 (b).

TABLE II
Nonisothermal Crystallization Kinetic Parameters Obtained from Jeziorny Method

ϕ (°C/min)	n	Z_t (10^{-6})	Z_c	$t_{1/2}$ (min)	ΔE (kJ/mol)
iPP					
2.5	1.83	0.55	0.003	14.17	239.7
5	1.73	1.62	0.070	7.84	
10	1.79	2.91	0.280	4.16	
20	1.71	6.02	0.549	2.33	
40	2.19	3.64	0.731	1.29	
iPP/SiO_2					
2.5	1.68	1.12	0.004	12.62	260.3
5	1.57	2.54	0.076	6.97	
10	2.01	1.91	0.268	3.92	
20	1.87	4.94	0.543	2.09	
40	2.12	5.32	0.739	14.17	
co-PP					
2.5	1.42	1.30	0.004	14.03	241.5
5	1.41	2.86	0.078	7.88	
10	1.48	4.14	0.290	4.28	
20	1.28	2.45	0.525	2.22	
40	1.72	7.83	0.745	1.22	
co-PP/SiO_2					
2.5	1.66	0.87	0.004	18.42	215.9
5	1.55	1.71	0.070	9.92	
10	1.58	4.92	0.295	5.31	
20	1.50	9.53	0.562	2.91	
40	1.81	9.32	0.749	1.17	

neous nucleation effect but also will restrict nucleation of the crystallizing polymer. Furthermore, there is a relationship between the three-dimensional work of nucleation A and the parameter B:

$$A = nT_m^0 B \tag{6}$$

where n is the Avrami exponent. So, the following relationship holds[19,20]:

$$\varepsilon = \frac{A_f}{A_0} = \frac{n_f T_{m,f}^0 B_f}{n_0 T_{m,0}^0 B_0} \tag{7}$$

B can be derived from the slope of the linear curve of log ϕ versus $1/2.3\Delta T_p^2$. n_0 and n_f are the average value of Avrimi index of PP and its composite, respectively.

The equilibrium melting temperatures of iPP and *co*-PP composites were calculated by using Hoffman-Weeks method.[21] iPP and *co*-PP composites underwent isothermal crystallization at different temperatures in the range of 120–130°C. After complete crystallization, these composites underwent subsequent heating until complete melting at the heating rate of 10°C/min. To each isothermal crystallization temperature (T_c), there is a corresponding melting temperature (T_m). T_m^0 can be determined from the intersect between a linear regression line drawn through the bulk of the $T_m - T_c$ data and the $T_m = T_c$ line. The equilibrium melting temperatures of iPP, *co*-PP, and their composites are listed in Table III.

TABLE III
The Equilibrium Melting Temperatures of iPP, *co*-PP, and their Composites

Samples	T_m^0 (°C)
iPP	188.8
iPP/SiO_2	183.0
co-PP	160.3
co-PP/SiO_2	172.8

Figure 8 shows the plots of log ϕ versus $1/2.3\Delta T_p^2$ for iPP, *co*-PP, and their composites. The slope is 3.4 $\times$ 10^4 for iPP, 2.3 $\times$ 10^4 for iPP/SiO2, 0.6 $\times$ 10^4 for *co*-PP, and 2.5 $\times$ 10^4 for *co*-PP/SiO_2. Thus, the nucleation activities of SiO_2 are 0.67 in iPP/SiO_2 and 4.58 in *co*-PP/SiO_2. The results show that SiO_2 is an effective nucleating agent for iPP, but restrains the nucleation of *co*-PP.

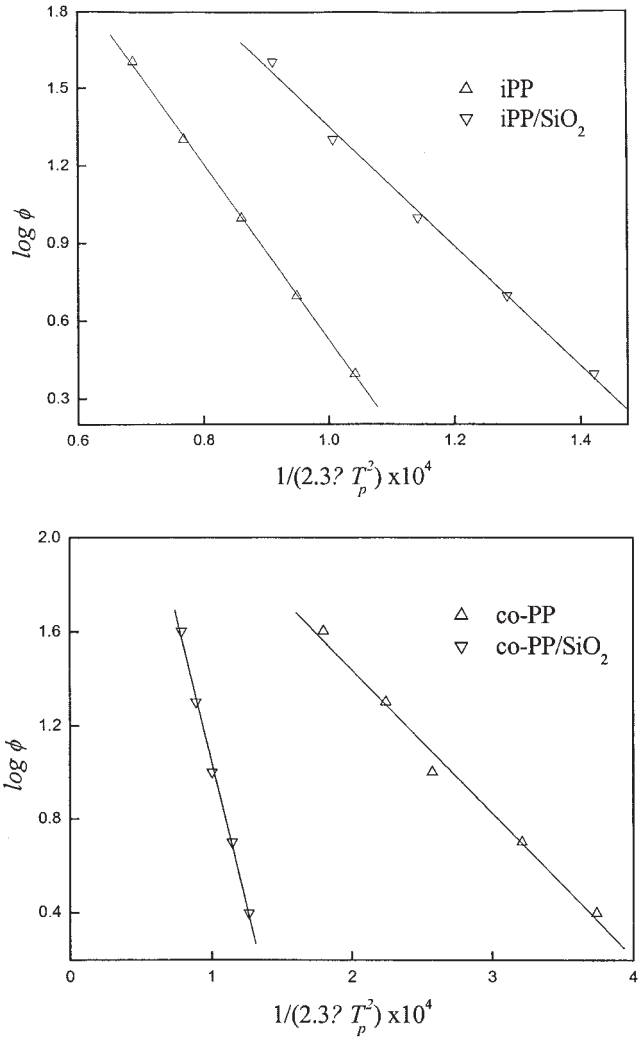

Figure 8 Plots of log ϕ versus $1/2.3\Delta T_p^2$ for iPP, *co*-PP, and their composites.

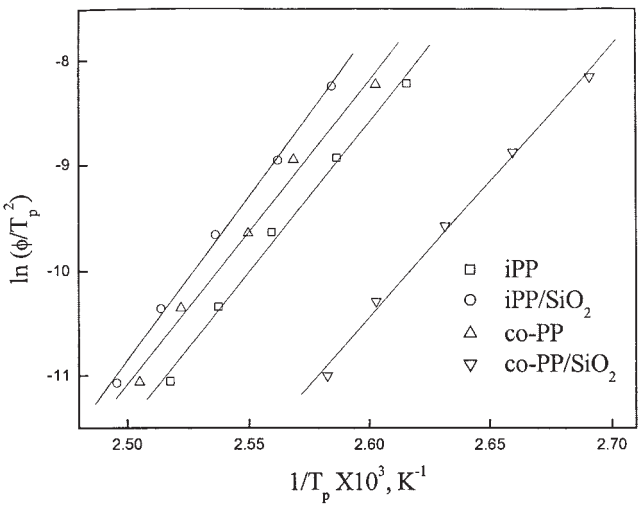

Figure 9 Plots of $\ln(\phi/T_p^2)$ versus $1/T_p$ for iPP and *co*-PP samples.

Activation energy

Considering the influence of the various cooling rate on the nonisothermal crystallization process, Kissinger[22] suggested a method to determine the activation energy (ΔE) for the transport of the macromolecular segments to the growing surface by calculating the variation of T_p with the cooling rate ϕ.

$$\frac{d[\ln(\phi/T_p^2)]}{d(1/T_p)} = \frac{-\Delta E}{R} \tag{8}$$

where R is the gas constant. T_p is the peak temperature of crystallization. Plots of $\ln(\phi/T_p^2)$ versus $1/T_p$ are shown in Figure 9. Activation energy derived from the slope of the line is 239.7 kJ/mol for iPP, 260.3 kJ/mol for iPP/SiO_2, 241.5 kJ/mol for *co*-PP, and 215.9 kJ/mol for *co*-PP/SiO_2.

The iPP/SiO_2 has higher activation energy than the iPP, indicating the crystal growth of iPP/SiO_2 composite is more difficult. The *co*-PP/SiO_2 has lower activation energy than the *co*-PP, indicating crystal growth of *co*-PP/SiO_2 composite is easier. ΔH_c (Table I) of all the composites can explain the changes of crystal growth rate. Because crystal growth is more difficult in iPP/SiO_2 composite, the iPP/SiO_2 composite has lower ΔH_c than iPP at the same cooling rate. Because crystal growth is easier in the *co*-PP/SiO_2 composite, the *co*-PP/SiO_2 composite has higher ΔH_c than *co*-PP at the same cooling rate.

Crystallization of polymers contains two steps: nucleation and crystal growth. Crystallization rate is controlled by the step with slower speed rate. Crystallization rates of PP and PP composites depend on the nucleation. The iPP/SiO_2 has higher nucleation and lower crystal growth rate than iPP. This indicates that the crystallization rates of iPP and iPP/SiO_2 are controlled by the nucleation. The *co*-PP/SiO_2 has lower nucleation and higher crystal growth rate than *co*-PP. This indicates that the crystallization rates of *co*-PP and *co*-PP/SiO_2 are controlled by the nucleation.

Crystal structure

It is well known that PP mainly has three crystalline forms: monoclinic α, hexagonal β, and orthorhombic γ.[11] Figure 10 shows the WAXD patterns of iPP, *co*-PP, and their composites. The two diffractograms in Figure 10(a) indicate that neat iPP and iPP/SiO_2 crystallize primarily in the monoclinic α form via reflections at 2θ = 13.7, 16.5, 18.1, and 21.1° corresponding to (110), (040), (130), and (111) crystal plane, respectively.[23] The diffractogram of neat iPP also reveals that the presence of the hexagonal β form via reflections at 2θ = 15.6° corresponding to (300) crystal plane. While the diffractogram of iPP/SiO_2 shows that the presence of SiO_2 nanoparticle strongly decreases the peak intensity of the (300) crystal plane, the relative proportion of the β form was determined by the following equation[24]:

$$k_\beta = \frac{I_\beta}{I_\beta + I_{\alpha1} + I_{\alpha2} + I_{\alpha3}} \tag{9}$$

where I_β is the intensity of the (300) peak, and $I_{\alpha1}$,$I_{\alpha2}$, and $I_{\alpha3}$ are the intensities of the (110), (040), and (130) peaks of the α form, respectively. Similarly, the relative proportion of the three α forms can be calculated. The results are listed in Table IV.

$$k_{\alpha1} = I_{\alpha1}/(I_\beta + I_{\alpha1} + I_{\alpha2} + I_{\alpha3}) \tag{10}$$

$$k_{\alpha2} = I_{\alpha2}/(I_\beta + I_{\alpha1} + I_{\alpha2} + I_{\alpha3}) \tag{11}$$

$$k_{\alpha3} = I_{\alpha3}/(I_\beta + I_{\alpha1} + I_{\alpha2} + I_{\alpha3}) \tag{12}$$

The data in Table IV indicate that the presence of SiO_2 nanoparticles results in a great decrease of the relative proportion of hexagonal β form, from 32.8 to 15.3%. With the addition of SiO_2 nanoparticles, the relative proportions of the three monoclinic α forms increase, especially the (040) crystal plane. The SiO_2 nanoparticles restrain crystallization of β form of iPP. At the same time, the SiO_2 nanoparticles induce iPP to crystallize directionally along the *b* axis.

There is no β crystalline form in *co*-PP (Fig. 10(b)). The relative proportions of (110), (040), and (130) crystal plane can be calculated according to the method mentioned earlier, and the results are listed in Table IV. Different from iPP, the crystalline form and relative proportions of the three α forms of *co*-PP do not

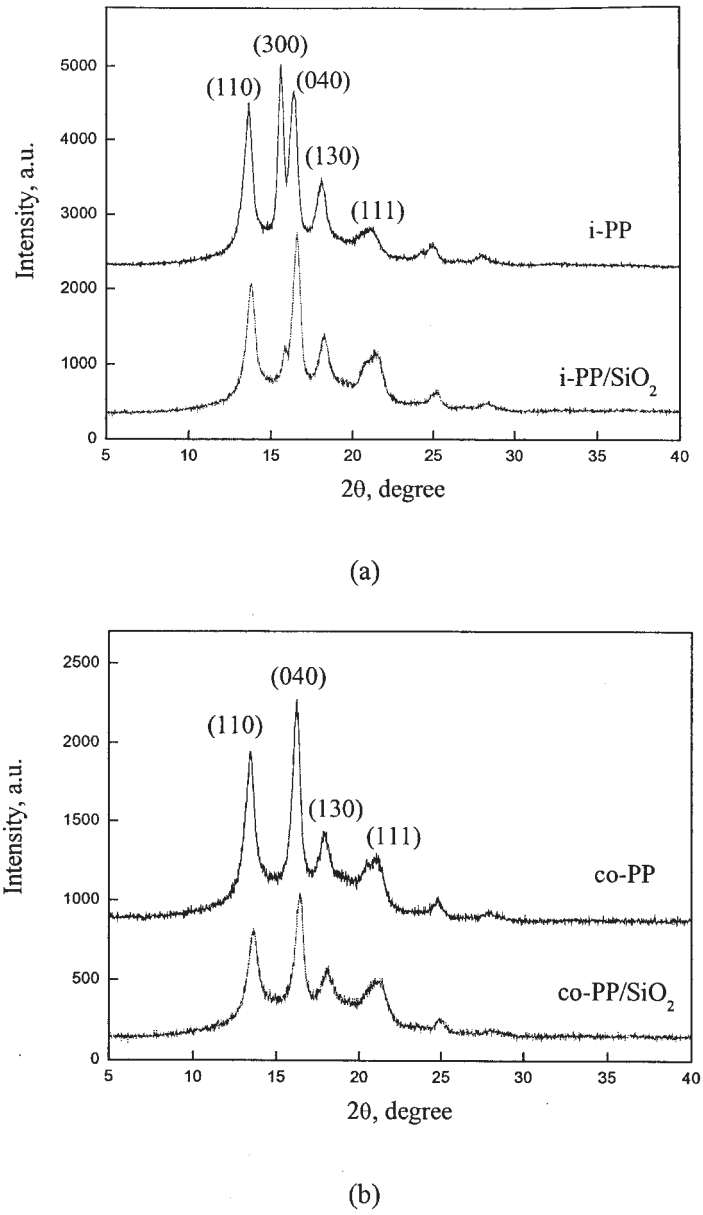

Figure 10 X-ray diffractions of iPP, *co*-PP, and their composites.

change much with the addition of SiO_2 nanoparticles (Table IV).

CONCLUSIONS

The crystallization and melting behavior of iPP and *co*-PP containing SiO_2 nanoparticles were investigated by DSC. SiO_2 moderately increased the crystallization temperature of iPP from 117.7 to 121.3°C at the cooling rate of 10°C/min and shortened the half crystallization time. However, SiO_2 greatly decreased the crystallization temperature of *co*-PP from 119.2 to 107.0°C at the cooling rate of 10°C/min and prolonged the half crystallization time. A modified Avrami theory was successfully used to well describe the early stages of nonisothermal crystallization of iPP, *co*-PP, and their composites. SiO_2 exhibited active nucleation for iPP, but showed little nucleation activity for *co*-PP and even restrained the nucleation. iPP/SiO_2 composite had higher activation energy than iPP, indicating the difficulty of crystal growth of the composite. *Co*-PP/SiO_2 composite had lower activation energy than *co*-PP, indicating the ease of crystal growth of the composite. Crystallization rates of

TABLE IV
Analyses of Crystal Structure of iPP, *co*-PP, and their Composites

Samples	$K_{\alpha 1}$	$K_{\alpha 2}$	$K_{\alpha 3}$	K_{β}
iPP	0.265	0.258	0.149	0.328
iPP/SiO_2	0.280	0.387	0.179	0.153
co-PP	0.351	0.455	0.194	—
co-PP/SiO_2	0.335	0.442	0.223	—

PP and PP composites depended on the nucleation. Because of its high nucleation rate, the iPP/SiO_2 composite had higher crystallization rate than iPP. Because of its low nucleation, the *co*-PP/SiO_2 composite had lower crystallization rate than *co*-PP. With the addition of SiO_2 nanoparticles, the relative proportions of the three monoclinic α forms increase, especially the (040) crystal plane of iPP. The SiO_2 nanoparticles restrain crystallization of β form of iPP. Different from iPP, the crystalline form and the relative proportions of the three α forms of *co*-PP do not change much with the addition of SiO_2 nanoparticles.

References

1. Xie, X. L.; Liu, Q. X.; Li, Y.; Zhou, X. P.; Zhang, Q. X.; Yu, Z. Z.; Mai, Y. W. Polymer 2004, 45, 6665.
2. Zhang, W. A.; Chen, D. Z.; Zhao, Q. B.; Fang, Y. E. Polymer 2003, 44, 7953.
3. Shelley, J. S.; Mather, P. T.; Devries, K. L. Polymer 2001, 42, 5849.
4. Hu, Y. H.; Chen, C. Y.; Wang, C. C. Polym Degrad Stab 2004, 84, 545.
5. Musto, P.; Ragosta, G.; Scarinzi, G.; Mascia, L. Polymer 2004, 45, 1697.
6. Chung, M. J.; Jang, L. W.; Shim, J. H.; Yoon, J. S. J Appl Polym Sci 2005, 95, 307.
7. Brown, J.; Rhoney, I.; Pethrick, R. A. Polym Int 2004, 53, 2130.
8. Wu, D. Z.; Wang, X. D.; Song, Y. Z.; Jin, R. G. J Appl Polym Sci 2004, 92, 2714.
9. Chan, C. M.; Wu, J. S.; Li, J. X.; Cheung, Y. K. Polymer 2002, 43, 2981.
10. Rong, M. Z.; Zhang, M. Q.; Zheng, Y. X.; Zeng, H. M.; Friedrich, K. Polymer 2001, 42, 167.
11. Zhang, Q. X.; Yu, Z. Z.; Xie, X. L.; Mai, Y. W. Polymer 2004, 45, 5985.
12. Mubarak, Y.; Harkin-Jones, E. M. A.; Martin, P. J.; Ahmad, M. Polymer 2001, 42, 3171.
13. Qian, J. S.; He, P. S.; Nie, K. J Appl Polym Sci 2004, 91, 1013.
14. Li, J.; Zhou, C. X.; Wang, G. Polym Test 2003, 22, 217.
15. Jeziorny, A. Polymer 1978, 19, 1142.
16. Kissinger, H. E. J Res Natl Stand, 1956, 57, 217.
17. Janigova, I.; Chodak, I. Eur Polym J 1995, 31, 271.
18. Dobreva, A.; Gutzow, I. J Non-crystalline Solids 1993, 1, 162.
19. Dobreva, A.; Gutzow, I. J Non-crystalline Solids 1993, 13, 162.
20. Hoffman, J. D.; Robert, L. M. Polymer 1997, 13, 3151.
21. Tang, J. G.; Wang, Y.; Liu, H. Y.; Belfiore, L. A. Polymer 2004, 45, 2081.
22. Torre, F. J.; Cortazar, M. M.; Gomez, M. A.; Ellis, G. Polymer 2003, 44, 5209.
23. Cho, K.; Li, F.; Choi, J. Polymer 1999, 40, 1719.
24. Zhang, F. J.; Gong, Y. M.; He, T. B. Eur Polym J 2003, 39, 2315.